Optical measurement of adipose tissue thickness and comparison with ultrasound, magnetic resonance imging, and callipers

Dmitri Geraskin
Heide Boeth
Matthias Kohl-Bareis
University of Applied Sciences Koblenz
RheinAhrCampus
Suedallee 2
Remagen, 53424
Germany

Abstract. Near-infrared spectroscopy is used to quantify the subcutaneous adipose tissue thickness (ATT) over five muscle groups (vastus medialis, vastus lateralis, gastrocnemius, ventral forearm and biceps brachii muscle) of healthy volunteers (n=20). The optical lipid signal (OLS) was obtained from the second derivative of broad band attenuation spectra and the lipid absorption peak (λ=930 nm). Ultrasound and MR imaging as well as mechanical calliper readings were taken as reference methods. The data show that the OLS is a good predictor for ATT (<16 mm) with absolute and relative errors of <0.8 mm and <24%, respectively. The optical method compares favourably with calliper reading. The finding of a non-linear relationship of optical signal vs. ultrasound is explained by a theoretical two-layer model based on the diffusion approximation for the transport of photons. The crosstalk between the OLS and tissue hemoglobin concentration changes during an incremental cycling exercise was found to be small, indicating the robustness of OLS. Furthermore, the effect of ATT on spatially-resolved spectroscopy measurements is shown to decrease the calculated muscle hemoglobin concentration and to increase oxygen saturation.
[DOI: 10.1117/1.3184425]

Keywords: near-infrared spectroscopy; lipid; adipose tissue thickness; monitoring; muscle oxygenation.

Paper 09027R received Jan. 30, 2009; revised manuscript received May 11, 2009; accepted for publication Jun. 2, 2009; published online Jul. 27, 2009.

1 Introduction

Near-infrared spectroscopy (NIRS) has been used for a number of years as a noninvasive tool for the quantification of muscular oxygenation (e.g., see reviews in Refs. 1–3). It relies on the low absorption of biological tissue for wavelengths in the range 600 to 1000 nm, which permits a photon penetration deep enough to probe muscular tissue and therefore supplies information of hemoglobin (and myoglobin) concentration and its oxygenation during exercise. Different methodological approaches have been followed to quantify hemoglobin concentration based on continuous wave, time-, or frequency-domain spectroscopy at a number of wavelengths in conjunction with models for the transport of photons in tissue (e.g., Refs. 4 and 5). Most NIRS monitoring systems are based on a few source and detector positions only, and therefore it is difficult to discern, measure, or discriminate between different tissue sections. Consequently, the underlying models to convert spectroscopic data into hemoglobin concentrations assume a homogeneous tissue with bulk optical properties of absorption and scattering. It is obvious that for muscular tissue this assumption is wrong, and skin and especially subcutaneous fat has to be taken into account. Experimentally, it has been pointed out before that the calculated hemoglobin changes correlate with the adipose tissue thickness (ATT), i.e., the subcutaneous fat layer that consists predominantly of lipid.[6–8] The effect of layered structures on reflectance data has been described and analyzed by experiments using tissue simulating phantoms and mathematical models.[9–15]

The broader purpose of this work is to provide the background for improvement of NIRS methodology. Here we expand on a preliminary report[16] with the objective to quantify the lipid content of the subcutaneous layer (ATT), and a description within a theoretical model. In a second step this knowledge of the ATT can be applied for a correction of NIRS algorithms for the conversion of spectroscopic data into hemoglobin concentrations of muscular tissue.[17] This is, however, beyond the scope of this work.

NIRS has been applied before for the quantification of body lipid content, with focus either on subcutaneous fat, on total body fat, or selected tissues. Conway, Norris, and Bodwell[18] demonstrated that lipid in tissue can be quantified by analysis of its absorption peak close to 930 nm in broadband attenuation spectra, and that this correlates with total body fat. A commercial optical body fat analyzer (Futrex 5000

Address all correspondence to: Matthias Kohl-Bareis, University of Applied Sciences Koblenz, RheinAhrCampus, Suedallee 2, 53242 Remagen, Germany; Tel.: +44(0) 2642 932 342; Fax: +44(0) 2642 932 399; E-mail: kohl-bareis@rheinahrcampus.de

1083-3668/2009/14(4)/044017/12/$25.00 © 2009 SPIE

and 6100, Futrex Incorporated Hagerstown, Maryland) has been developed based on the attenuation data at two or six wavelengths in the NIR region, and promises to calculate total body fat. Studies have been published to evaluate its performance either for ATT or whole body fat measurements. Fuller, Dewit, and Wells[19] compared skin fold thickness with optical signals and concluded that the data were insufficient to fully decide the usefulness of the Futrex system. Kalantar-Zadeh et al.[20] compared NIRS lipid signals as measured by the Futrex 5000 with skin folds on the biceps and found poor correlation (correlation coefficient $R=0.55$). Another study showed that the same system performed not better than skin fold or ultrasound measurements in the assessment of either subcutaneous or total body fat.[21] Furthermore, the system was evaluated to estimate total body fat with the conclusion that the skin fold data (calliper) is more accurate as a predictor.[22] On a similar line, Schreiner et al.[23] found that the device offers little advantage in reliability over conventional measures (weight, size, height, etc.) for an estimation of the body mass index (BMI). Hicks et al.[24] reported that body fat is reliably estimated in only two of three subjects. In another study it was concluded that the Futrex 6100 produced unacceptable data quality for percent body fat estimations.[25] There are more reports published with similar outcomes on this ambitious goal to use the optical signal as a predictor of total body lipid content.[26–29] A different optical device has been developed based on reflectance measurements at three distances with one wavelength (660 nm), and a better correlation of optical data with body fat and electrical impedance data was found.[30–32] Other thorough spectroscopic approaches based on time-domain or diffuse optical imaging focused on the simultaneous quantification of lipid and hemoglobin or water in tissue.[33–35]

For a full understanding of optical fat measurement, the transport of photons in highly scattering media like tissue has to be considered and included. The theoretical analysis of the effect of layered structures on optical data has been dealt with in a number of publications (e.g., Refs. 7, 10, 36, and 37). Most of this work utilizes Monte Carlo simulations (MCS) for the calculation of photon reflectance, absorption, or optical path length depending on tissue geometry and the optical properties (absorption coefficient μ_a, transport scattering coefficient μ_s', refractive index n). To overcome the long computational time inherent to MCS, Kienle et al.[38,39] developed an analytical solution for the reflectance of a homogeneous two-layer structure.

In this work we readdress the quantification of ATT by near-infrared spectroscopy and try to tie this topic up both from the experimental and model perspective. The outline of this work is as follows: We show by comparison and correlation with ultrasound, standard calliper readings, and magnetic rasonance imaging (MRI) that ATT can be predicted with optical means. To that end we compare optical data acquired over five different muscle groups of healthy subjects. A theoretical model of layered structures for the light transport in tissue is exploited to predict the lipid signal in the optical spectra, and to explain the observed nonlinear relationship of optical and reference data. In addition, this model allows the sensitivity and errors to be estimated depending on the source-detector distance of the optical measurement and the tissue optical properties. For NIRS monitoring of muscle oxygenation, two further aspects are important that are analyzed both in experiment and model. We show that the crosstalk of the optical lipid signal with hemoglobin changes in the tissue is small, and further report on the influence of the ATT on the measured hemoglobin parameters.

2 Methods

The spectroscopy system is based on a Peltier-cooled slow-scan charge-coupled device (CCD) camera (Spec-10, Roper Scientific, Princeton Instruments, Trenton, New Jersey) with a 1340×400 pixel detector array and 16-bit resolution in combination with a spectrometer (SP-150, Acton Research, Acton, Massachusetts) with a diffraction grating of 300 grooves/mm and a blaze wavelength of 750 nm, resulting in an overall detection range between 550 and 1000 nm. Six light-detecting fiber bundles of 1 mm diam were arranged in a line separated by $\Delta\rho=2.5$ mm at a mean distance $\rho=35$ mm from the light delivering bundle (5 mm diam). The detection bundles were connected to the input slit of the spectrometer with a separation of 0.5 mm to clearly separate the six independent spectra recorded. The output of a standard 50-W halogen light source was focused with a condensor optic into the light-delivering-fiber bundle. An integrating sphere of 8 in. diam (IS-080-SF, Labsphere Incorporated, Estacada, Oregon) served as a normalization standard. The acquisition rate was typically 0.4 Hz. A pixel binning of 10 was set for the horizontal (wavelength) axis of the CCD chip, while for its vertical axis the binning was selected to include the pixels illuminated by each fibre. Count rates were typically in the range of 5000 s^{-1} $pixel^{-1}$ (including binning) for each fiber. Data acquisition and on-line analysis of the spectra was programmed in Labview 7.1 (National Instruments Incorporated, Austin, Texas) based on the driver package SITK (Roper Scientific, USA) giving full control of all camera functions as well as an on-line evaluation. All raw spectra were stored for additional and independent off-line data evaluation in Matlab (Version R2006b; Mathworks Incorporated, Natick, Massachusetts). The wavelength dependence of the recorded reflected light intensities I_i (index $i=1$ to 6 signifying the detector) was corrected by the reference spectra $I_{\mathrm{ref},i}(\lambda)$ recorded with the integrating sphere and converted into attenuation spectra,

$$A_i(\lambda)=\log_{10}[I_{\mathrm{ref},i}(\lambda)/I_i(\lambda)]. \quad (1)$$

The resolution of the spectrometer system was about 10 nm. For the quantification of the lipid content, the attenuation spectra [unit is optical density (OD)] for the distances $\rho=29$, 31.5, and 34 mm were averaged. The larger source–detector distances of 36.5, 39, and 41.5 mm were ignored, as in some cases the lower light intensity resulted in larger errors of the optical lipid signal (OLS).

Optical reflectance spectra, ultrasound measurements, and calliper skin fold readings were collected from 20 volunteers (10 male; age 26 (±2.7) yrs, height 181 (±8) cm, body weight 76 (±6) kg; and 10 female, age 24 (±2.7) yrs, height 171 (±8) cm, body weight 63 (±7) kg). For each volunteer, data were sampled on the skin over five muscle groups (gastrocnemius, musculus vastus lateralis, musculus

vastus medialis, forearm muscle, and biceps branchii muscle), both on left and right hemispheres. Additionally, the forearm readings were repeated with the arm held in a vertical position over the head to induce changes in hemoglobin concentration. This gave a total of 240 samples from 200 sites. The optical spectra were collected for about 60 sec and averaged. Optical spectra and ultrasound images (SonoSite 180, 5-MHz Linear Transducer, SonoSite Incorporated, Bothell, Washington) were taken from the same sites. As the pressure of the ultrasound transducer might affect the lipid thickness reading, the ultrasound-measured ATT_{US} thickness was taken from three independent images and averaged. Calliper measurements were taken from the skin fold thickness at the sites of light interrogation with a standard calliper (Slim Guide Skinfold Caliper, Creative Health Products, Plymouth, Michigan), with calliper skin thickness (CST) being half these values. All calliper readings were taken by the same person, with the volunteers seated in a relaxed position with a 90-deg flexion at the knee joint and the arm resting on a table. From the 200 sample sites and 240 readings, 182 calliper readings could be obtained. For the remaining positions (58 corresponding to 24.2%), the tissue elasticity was not high enough to allow a reading with the mechanical calliper. These 58 sites separate for the different muscles groups: forearm 0, biceps brachii 0, vastus lateralis 17, vastus medialis 22, and gastrocnemius 19 (with 40 sites per muscle group). To check this high failure rate, a second, independent calliper reading was taken in selected volunteers, which did not improve the data.

MRI images of three subjects [age 27 ($\pm$3.2) yrs, height 170 ($\pm$8) cm, body weight 63 ($\pm$14) kg] were obtained using a MR scanner operating at 0.5 T field strength (T5 II, Philips, Netherlands). A spin-echo sequence (TR=600 ms, TE=20 ms) was employed to acquire 16 images of 5-mm slice thickness. To that purpose, the thigh and calf of volunteers was placed into a dedicated knee–receive–coil. Vitamin E pills served as anatomical markers for the placement of the optical fibers. The adipose thickness ATT_{MR} was read by visual inspection of the MRIs images and compared with the OLS. Six to nine measurements were taken for both thigh and calf, giving a total of 46 measurements for three subjects.

Additionally, 18 datasets from 8 volunteers [4 male, age 29.3 ($\pm$5.4) yrs, height 187 ($\pm$11) cm, body weight 75 ($\pm$9.0) kg; 4 female, age 29.5 ($\pm$10.3) yrs, height 168 ($\pm$3) cm, body weight 63 ($\pm$6) kg] acquired during incremental cycling exercise under hypoxic conditions were reanalyzed (for details see Geraskin et al.[40]). In this study, the thigh (vastus lateralis muscle) was monitored for four hours with three periods of incremental cycling power (steps of ΔP =30 W up to maximal power) under normoxic or altitude conditions of 2000 and 4000 m (oxygen concentrations of 21.0, 15.4, and 11.9% in the inhaled air). Maximal exercise power and hypoxic conditions resulted in large changes in hemoglobin concentrations and a strong desaturation, and therefore this served to test for possible crosstalk from hemoglobin absorption to the optical lipid measurements. For these volunteers, ultrasound ATT_{US} was measured as well (Vivid 3, 739 L Superficial, General Electric).

All subjects provided their informed consent and were aware that they were free to terminate the testing at any time without consequence for doing so.

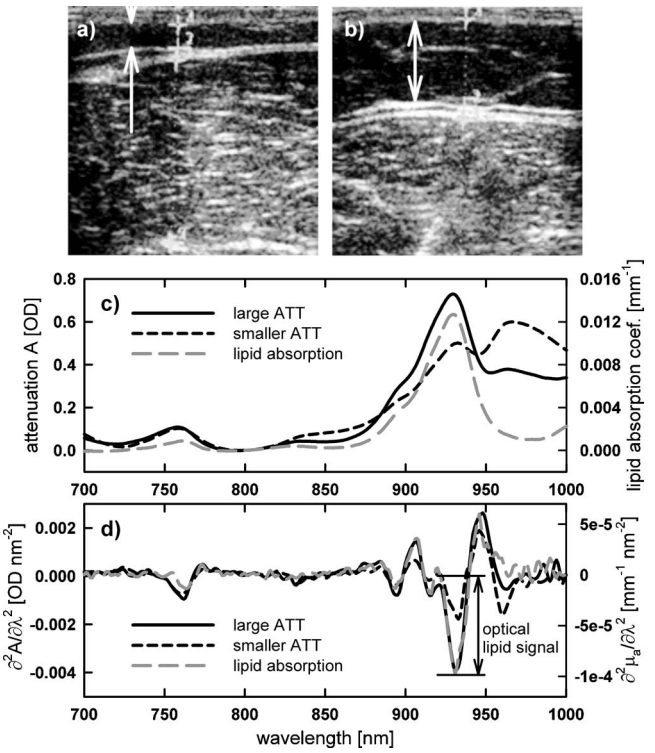

Fig. 1 Ultrasound images of the tissue over the vastus laterals muscle with lipid layers marked by arrows (a) with a thickness ATT_{US} =3 mm and (b) ATT_{US}=11.4 mm. (c) Attenuation spectra normalized at 800 nm measured for the tissue shown in (a) and (b). For comparison, the absorption spectrum of pure lipid[41] (right-hand scale) is shown. (d) Second differential with respect to λ of the spectra in (c). The optical lipid signal OLS is here defined as the magnitude of $\partial^2 A/\partial\lambda^2$ at 930 nm.

In Figs. 1(a) and 1(b), ultrasound images from two volunteers are shown that were measured over the vastus lateralis muscle. The adipose tissue layer is revealed as a region of low signal over the muscular tissue with its more complex structure in the images. In Fig. 1(c), two attenuation spectra are depicted, measured for the same tissues shown in Figs. 1(a) and 1(b) by averaging the attenuation for source–detector distances at ρ=29.0, 31.5, and 34.0 mm. In the spectra, the prominent absorption of deoxygenated hemoglobin deoxyHb ($\lambda \approx 760$ nm) and water ($\lambda \approx 970$ nm) are apparent. The strong peak close to 930 nm coincides with the absorption of pure lipid[41] [dashed line in Fig. 1(c)]. As the adipose tissue has a low water content, the water absorption band is more pronounced for the tissue with smaller ATT.

The first objective is to estimate the tissue lipid content from the optical spectra. To this end the second derivative of the attenuation spectra with respect to the wavelength was calculated and smoothed over an effective bandwidth of 3 nm. In Fig. 1(d) this is shown for the spectra of Fig. 1(c). In these spectra, the signal of the lipid absorption is the prominent feature, and the optical lipid signal OLS is taken as the magnitude of these spectra at 930 nm. To account for noise in the spectra, the magnitude within a bandpass of 7 nm was considered:

$$\mathrm{OLS} = \max\left[\left|\frac{\partial^2 A}{\partial \lambda^2}\right| (927\ \mathrm{nm} - 933\ \mathrm{nm})\right]. \quad (2)$$

OLS is given in units of $\mathrm{OD}\cdot\mathrm{nm}^{-2}$. The derivative spectrum is less sensitive to variations in tissue absorption that are not attributed to lipid, and therefore crosstalk from other tissue absorbers (mainly water and hemoglobin) is reduced. In an independent approach, the lipid signal was estimated from the area of the derivative spectra: however, this proved to be less reliable with increased variations and residue when compared with ultrasound, and was therefore discarded.

For the calculation of the oxygenation parameters, the spatially resolved spectroscopy (SRS) approach was followed, which calculates tissue absorption spectra $\mu_a(\lambda)$ from the slope of attenuation ΔA with source-detector distance $\Delta\rho$.[42–44,40]

$$\mu_a(\lambda) = \frac{1}{\mu_s'(\lambda)} \cdot \frac{1}{3} \cdot \left[\ln(10)\frac{\Delta A(\lambda)}{\Delta\rho} - \frac{2}{\rho}\right]^2. \quad (3)$$

The transport scattering coefficient $\mu_s'(\lambda)$ is unknown but can be approximated from literature values.[45] For a wavelength range $720\ \mathrm{nm} < \lambda < 860\ \mathrm{nm}$, these absorption coefficient spectra were converted into hemoglobin concentrations for oxyHb and deoxyHb via matrix inversion by assuming that the absorption is dominated by hemoglobin with extinction coefficients,[46] referring to the hemoglobin molecule. The total hemoglobin concentration (tHb=oxyHb+deoxyHb) and oxygen saturation SO_2=oxyHb/tHb were subsequently calculated.

2.1 *Modeling*

To study and describe the reflectance of the tissue, the reflectance was modeled for a two-layered structure, where the upper layer mimics the adipose tissue (thickness ATT $\leqslant 16$ mm) and the lower layer represents muscle (infinite thickness). The main difficulty for any model is the selection of the appropriate absorption and scattering properties, expressed by μ_a and μ_s'.

In-vitro measurements by Simpson et al.[47] showed values of μ_s' in the range of 2 mm^{-1} for skin, 1.1 (± 0.3) mm^{-1} for adipose subdermis tissue, and 0.6 mm^{-1} for abdominal muscle. Similarly, Bashkatov et al.[48] report on μ_s' of adipose tissue and found *in-vitro* values in the range of 1.20 (± 0.35) mm^{-1} for the spectral range considered here. Van Veen et al.[41] measured the scattering coefficient of lipid prepared from pig lard with time-domain methods and reported values decreasing from 0.7 to 0.45 mm^{-1} for the wavelength range from 600 to 1100 nm. There are many data published of bulk optical properties *in vivo*, which differ widely, depending on the tissue interrogated, the experimental technique employed, and the analysis method used. Torricelli et al.[34] measured transport scattering coefficients in the range of about 0.8 to 0.9 mm^{-1} for the arm and slightly higher values for the abdomen. Casavola et al.[49] report values of μ_s' in the range of 0.5 mm^{-1} for arm measurements. Matcher, Cope, and Delpy[45] obtained scattering coefficients of about 0.68 (± 0.08) mm^{-1} for the forearm and 0.95 (± 0.07) mm^{-1} for calf at 800 nm. In all reports, μ_s' is slightly decreasing with wavelength.[34,45,47] Similarly, published values of the absorption coefficients of tissue vary widely. Van Veen et al.[41] provided, the absorption spectra of purified lipid [see Fig. 1(c)], which coincides well with *in-vitro* data.[47] Matcher, Cope, and Delpy[45] obtained absorption coefficients of about 0.023 (± 0.004) mm^{-1} for the bulk tissue of the forearm and 0.017 (± 0.005) mm^{-1} for calf at 800 nm. This is in line with other work.[34,50]

Based on these literature values, the following parameters were chosen for the simulations, with μ_a and μ_s' set independently for muscle (index M) and lipid (index L) layers: $\mu_{a,M}$=0.005, 0.01, and 0.02 mm^{-1}, and $\mu_{s,M}'$=0.7, 1.0, and 1.3 mm^{-1}. The same scattering properties were used for the lipid layer ($\mu_{s,L}'$). The wavelength-dependent absorption coefficient of the lipid layer $\mu_{a,L}$ was taken from the spectra of pure lipid $\mu_{a,\mathrm{lipid}}$ [Fig. 1(c)], assuming that the adipose tissue layer is pure lipid.[41] To account for additional chromophores, an additional offset $\mu_{a,\mathrm{Loffset}}$ between 0.0 and 0.006 mm^{-1} in steps of 0.002 mm^{-1} was included: $\mu_{a,L}=\mu_{a,\mathrm{lipid}}+\mu_{a,\mathrm{Loffset}}$. Therefore, all parameters besides $\mu_{a,L}$ were assumed to be wavelength independent. The refractive index was set to n =1.4 for both layers. Reflectance was calculated for source–detector distances ρ up to 45 mm.

To compare the experimental OLS data with the simulations, reflectance spectra were calculated for the range 850 to 970 nm by inclusion of the spectra $\mu_{a,\mathrm{lipid}}(\lambda)$. These spectra were converted into attenuation spectra and analyzed as described for the experimental attenuation data, i.e., the second derivative with respect to wavelength was computed with the OLS obtained in analogy to Eq. (2). To mimic the finite spectral resolution of the experimental setup (about 10 nm), the simulated attenuation spectra were smoothed with a gliding average filter. Initially, a Monte Carlo model was employed for this calculation, which is rather computationally time consuming when reflectance spectra were required.[51] Finally, all calculations were done with an analytical solution for the two-layer model based on diffusion approximation.[38,39] For this purpose, an executable program was kindly provided by Kienle.[52] For a limited set of tissue parameters, the agreement of Monte Carlo and the analytical method was confirmed.

3 Results

3.1 *Experimental Lipid Measurements*

In Figs. 2–4, the correlation plots of the optical lipid signal OLS with ultrasound $\mathrm{ATT_{US}}$, calliper skin thickness (CST), and MRI-based $\mathrm{ATT_{MR}}$ are shown with ATT in the range from <1 to 16 mm. In Fig. 2(a), each point represents data from a single subject with different symbols for the five muscle groups. There is a clear nonlinear relationship between OLS and $\mathrm{ATT_{US}}$. For the estimation of prediction accuracy in the optical estimation of ATT, the data of Fig. 2(a) were fitted by the function

$$\mathrm{OLS} = p_1 \cdot [1 - \exp(-p_2 \cdot \mathrm{REF})]. \quad (4)$$

REF is $\mathrm{ATT_{US}}$ (or CST or $\mathrm{ATT_{MR}}$ for Figs. 3 and 4, respectively) with the fit parameters p_1 and p_2. The solid line of Figs. 2(a) and 2(b) represents this fit with p_1 =7.96110^{-3} $\mathrm{OD}\cdot\mathrm{nm}^{-2}$ and p_2=0.0966 mm^{-1} ($\mathrm{ATT_{US}}$ in units of millimeters). The residuum RES_i was calculated for

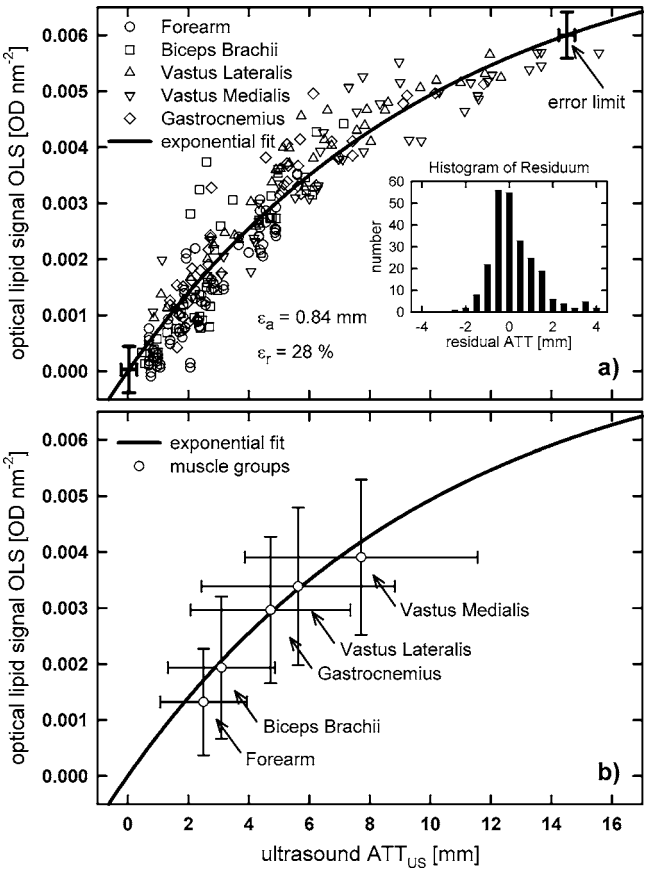

Fig. 2 Correlation of optical lipid signal (OLS) and ultrasound ATT_{US} for five different muscle groups on 20 subjects. The solid line represents an exponential fit (see text for details). (a) Data of all 20 subjects (insert: histogram of residuum with a mean of absolute residuum of 0.84 mm and mean relative error of 28%). The magnitudes of the experimental errors (see text for details) are plotted at the lower and upper end of the fitted curve. (b) Mean (±SD) values for the different muscle groups, with the same exponential fit as in (a).

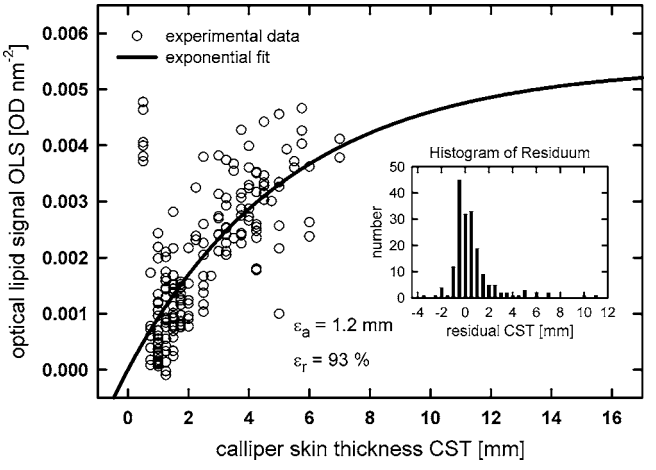

Fig. 3 Correlation of optical lipid signal (OLS) and calliper skin thickness (CST) for five different muscle groups of 20 subjects. The solid line represents a fit (see text). Insert: histogram of residuum with absolute and relative errors of 1.2 mm and 93%, respectively.

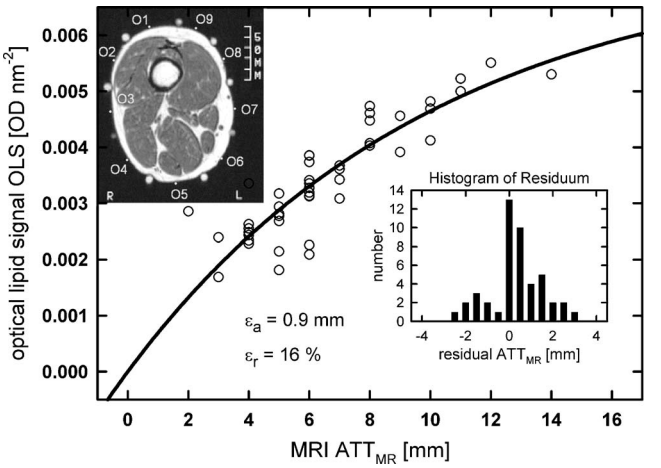

Fig. 4 Correlation of optical lipid signal (OLS) and MRI-based ATT_{MR}. The solid line represents an exponential fit (see text) of the experimental data. Right insert: histogram of residuum. Left insert: example of an MRI of the thigh with the bright outer lipid regions (thickness: 4 to 14 mm).

each data point (index i) as the difference between the experimental value of ATT_{US} and the fitted line. The histogram of RES is plotted in the insert of Fig. 2(a). To estimate the prediction errors, two values were considered. The mean magnitude of the residuum

$$\varepsilon_a = \langle |\mathrm{RES}| \rangle = \frac{1}{N}\sum_{i=1}^{N} |\mathrm{RES}_i|, \tag{5}$$

which gives an approximation of the absolute error, and the relative deviation

$$\varepsilon_r = \langle |\mathrm{RES}/\mathrm{ATT}_{\mathrm{US}}| \rangle. \tag{6}$$

For the data of Fig. 2(a), this analysis gave ε_a=0.84 mm and ε_r=28%.

To allow a comparison with published work, the correlation coefficient R was evaluated: when ATT_{US} was directly correlated with OLS, R=0.92 was obtained. Taking the nonlinearity into account by scaling ATT_{US} by Eq. (4) including p_1 and p_2, gave R=0.95.

When averaging the experimental data for each of the five muscle groups, the mean values (±SD) shown in Fig. 2(b) were obtained. There is a clear difference in mean ATT value for the different muscles with large intersubject variations. As can be expected, for the thigh (vastus lateralis and vastus medialis), the ATT is larger than for the calf (gastrocnemius) and the arm. The fitted line from the data of Fig. 2(a) correlates well with these mean values. The explanation for the nonlinear relationship between ATT_{US} and OLS can be found in the optical path length in the lipid layer, which depends both on its thickness and the underlying muscular tissue. A detailed analysis is presented next within the theoretical model. The error bars given at the lower and upper end of the ATT_{US} range of Fig. 2(a) are based on experimental uncertainties in determining the ultrasound and OLS (see next for details).

Table 1 Absolute and relative prediction errors (ε_a and ε_r) for the data shown in Figs. 2–4. In column 1 (OLS versus ATT_{US}), the whole dataset of 240 readings was included. Columns 2, 3, and 4 are based on the data where calliper readings could be obtained (see text for details). For column 5, an independent dataset was analyzed.

	1	2	3	4	5
Column:	OLS versus ATT_{US}		CST versus ATT_{US}	OLS versus CST	OLS versus ATT_{MR}
ATT [mm]	⩽16	0.75 to 7	0.75 to 7	0.75 to 7	2 to 14
ε_a [mm]	0.84	0.7	1.2	1.2	0.9
ε_r [%]	28	31	43	93	16

The same OLS data were correlated with calliper skin thickness (CST), which is shown in Fig. 3. CST is limited to the range ⩽7 mm, and as said in Sec. 2, no reading could be obtained for 24.2% of the samples. We have no explanation for this failure rate, but suspect that it is due to limitations in the calliper instrumentation and the underlying approach.

For a limited number of measurements, CST is small (<1 mm) with corresponding high OLS values. Again the data were fitted according to Eq. (4) (with $p_1 = 5.429 \cdot 10^{-3}$ OD·nm^{-2} and $p_2 = 0.1876$ mm^{-1}) giving the histogram of the residuum shown in the insert. The prediction errors are $\varepsilon_a = 1.2$ mm and $\varepsilon_r = 93\%$.

When taking a calliper reading it must be assumed that the sum of both skin and adipose tissue is measured. Therefore it seems obvious that an offset has to be included that takes into account the skin thickness. Equation (4) was therefore modified to include a third fitting parameter as offset, OLS $= p_1 \cdot [1 - \exp^{(-p_2 \cdot \mathrm{REF} - p_3)}]$. When fitting this function to the experimental data, no marked difference was obtained in terms of residuum and prediction errors ε_a and ε_r. Calliper CST and ATT_{US} were correlated (data not shown), and assuming that both measurements depend linearly on the lipid layer, a linear regression was fitted, giving prediction errors $\varepsilon_a = 1.2$ mm and $\varepsilon_r = 43\%$ (again, for the 75.8% of the samples where a reading could be obtained). To permit a better comparison of the methods, the optical lipid signal and ultrasound readings were evaluated (OLS versus ATT_{US}) for the same limited dataset, giving prediction errors of $\varepsilon_a = 0.7$ mm and $\varepsilon_r = 31\%$.

For the separate experimental dataset based on MRI, the correlation with OLS is shown in Fig. 4. An example MRI is shown in the insert where the nine vitamin E markers can be seen, and the approximate measurement positions for the optical spectra are numbered (O1 to O9). The regions rich in lipid are revealed by high signal intensity. The smallest ATT_{MR} values (2 mm) are larger than for the ATT_{US} data, as all measurements were taken from the leg [compare with Fig. 2(b)]. Fitting the data according to Eq. (4) (REF=ATT_{MR}) gives parameters $p_1 = 7.443 \cdot 10^{-3}$ OD·nm^{-2} and $p_2 = 0.0979$ mm^{-1}. The prediction errors are $\varepsilon_a = 0.9$ mm and $\varepsilon_r = 16\%$. The results of the prediction errors are summarized in Table 1.

3.2 *Estimation of Errors*

The prediction error ε_a of ATT based on the OLS is on the order of 0.7 to 1.2 mm, which brings up the question of experimental limitations for each measurement modality. The ATT_{US} values were generated by an analysis of three readings taken from three different images, with the mean of these three readings taken as ATT_{US} for each sample. The standard deviation of the three readings was also calculated, which had a mean of 0.26 mm when averaging over all samples. Similarly, for the optical attenuation spectra of the three detectors, the OLS was calculated independently with the mean plotted in Figs. 2–4. The standard deviation of OLS for the three detectors was evaluated for each measurement site that had a mean value of $4.14 \cdot 10^{-4}$ OD·nm^{-2}. These two mean values of the standard deviations represent a lower limit for the attainable residuum. In Fig. 2(a), these inherent experimental errors are plotted for two arbitrary points at the lower and upper ATT_{US} range of the fitted curve. It was tested whether this is the dominant error with the hypothesis that a larger standard deviation of the three independent measurements is correlated with a larger residuum. To this end, the standard deviation in the three OLS values was correlated with the residuum of Fig. 2(a) for all 240 samples. Similarly, the standard deviation of the three ultrasound readings was correlated with the residuum. These plots (data not shown) showed no clear correlation and therefore gave no indication that the residuum for the data of Fig. 2(a) is predominantly due to these experimental limitations.

The main limitation of the calliper readings is likely to be due to differences in tissue structure and composition that determine the mechanical properties, which is beyond the validation or assessment outlined here. The limited CST range (<7 mm) makes it difficult to compare the findings of CST versus ATT_{US} and OLS versus ATT_{US}. When taking ATT readings from the MRIs, similar errors for the ultrasound images resulted. Additional errors are likely to have occurred as the subjects had to be repositioned after taking MRIs in the MR coil to readings of optical spectra.

3.3 *Crosstalk of Optical Lipid Signal with Hemoglobin*

A further concern is that the hemoglobin concentration and oxygenation saturation of both the adipose and the muscle

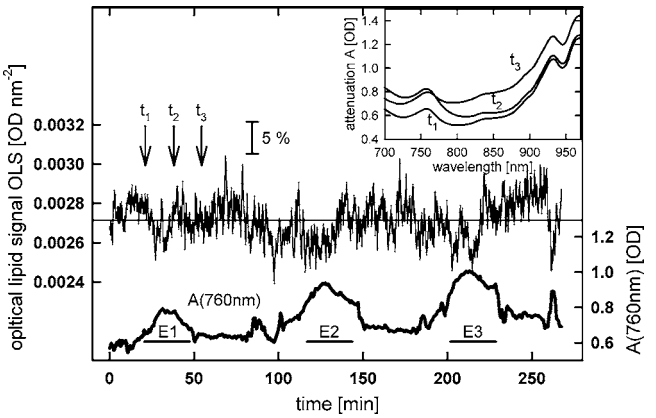

Fig. 5 Long-time monitoring of the OLS on the thigh (vastus lateralis) during three phases of an incremental exercise protocol separated by rest periods. The insert shows the attenuation spectra at three times (t_1, t_2, and t_3) during various stages of the exercise. At the bottom, the attenuation A for $\lambda = 760$ nm is shown (right-hand scale, with arbitrary offset). The exercise periods are marked by E1, E2, and E3 (corresponding to 21, 15.4, and 11.9% O_2 in inhaled air; see text for details).

tissue influence the OLS due to variations in the tissue attenuation spectra. To clarify this point experimentally, data acquired during an exercise protocol were reanalyzed. In Fig. 5, data from a four-hour period is shown monitoring oxygenation during incremental cycle exercise periods. The optical lipid signal has a mean value OLS=0.0027 OD·nm^{-2} with variations of about ±5%. The incremental exercise resulted in strong alterations of blood flow and oxygenation (for details see Geraskin et al.[40]) and subsequently in large attenuation changes. The time course of attenuation at 760 nm (see Fig. 5) varies by about 0.35 OD (corresponding to more than a factor of 2 in intensity) and 0.25 OD for $\lambda = 930$ nm. For three points in times t_1, t_2, and t_3 at various phases (power loads) of the first exercise period, the attenuation spectra are shown in the insert. There is no apparent correlation of OLS and attenuation. Similar variations in OLS were observed in 18 other datasets acquired during the same exercise paradigm [mean of ATT_{US} 5.5 (±3.5) mm]. The mean of the coefficient R for the correlation between OLS and A(760 nm) was 0.37 (±0.20). The coefficient of variation CV in OLS averaged over these 18 long datasets was 3.8 (±2.9)%. Based on the fitted line shown in Fig. 2, this variation of 3.8% in OLS corresponds to an uncertainty in ATT of about 0.17 mm (at ATT=4 mm). This number can be taken as an upper limit for the crosstalk of hemoglobin and OLS.

With a similar intent to check for a crosstalk of different blood concentrations, the measurement on the forearm were done twice with the arm in a lower position (about the height of the heart) and by holding the arm upward. When comparing the OLS readings during upper and lower positions, no significant difference in the OLS was observed.

3.4 *Influence of Adipose Tissue Thickness on Hemoglobin and SO_2*

For the 240 measurements, the hemoglobin parameters oxyHb, deoxyHb, tHb, and SO_2 were plotted as a function of ATT_{US} (Fig. 6), separately for each muscle group. There is a clear decrease in the concentrations and an increase in SO_2 with increasing ATT_{US} for all sites. This trend is different in quality, as expressed by the correlation coefficient and in the slope for the different muscle groups. The correlation of tHb and ATT_{US} is strongest for values derived from vastus lateralis and vastus medialis (R=0.93 and 0.79, respectively), while weak for the forearm. Similarly, the correlation of SO_2 and ATT_{US} is best for the large muscle groups of the thigh and lowest for the forearm.

3.5 *Comparison with Tissue Model*

The tissue model was employed to further shed light on the experimental findings with the objectives to explain the magnitude of the OLS and its nonlinear relationship with ATT, its dependence on source-detector distance ρ, and to estimate the influence of the optical properties of the tissue (μ_s', μ_a). Furthermore, the experimental condition of a finite bandwidth of the spectrometer has to be evaluated. Here the two-layer model described in Sec. 2 was employed with the upper and lower layer being lipid and muscle. In Fig. 7(a) the calculated optical lipid signal is plotted as a function of ATT with fixed, wavelength independent values $\mu_{a,M}=0.01$ mm^{-1}, $\mu_{s,L}'=1$ mm^{-1}, and $\mu_{s,M}'=1$ mm^{-1}. The absorption of the lipid layer $\mu_{a,L}$ is assumed to be that of pure lipid. It is apparent that the source-detector distance ρ has a strong influence on OLS. When ATT is small compared to ρ, OLS increases approximately linearly with ATT, while for ATT $>\rho/3$ it levels off. The form of this function reflects the dependence of OLS on the photon penetration into the tissue (depth sensitivity profile), which increases with ρ. As a consequence, when a lipid thickness of above 10 mm needs to be determined, a source-detector distance of ⩾25 mm is advisable. With a similar argument, optical measurements of thicker adipose layers are likely to have larger absolute errors when ρ is not appropriate.

To better compare the modeled functions with the experimental conditions, all further analysis was done by averaging the OLS signals for a detector geometry from ρ =29 to 34 mm. This is shown in Fig. 7(b), where the influence of the transport scattering coefficient is scrutinized. Scattering of lipid was varied between $\mu_{s,L}'=0.7$ mm^{-1} and 1.3 mm^{-1}, with the higher scattering giving a larger OLS. Again, this is explicable by the photon path length in lipid that scales with scattering. This is different from the muscle layer, where the effect of variations from $\mu_{s,M}'=0.7$ to 1.3 mm^{-1} is small, with the higher muscle scattering giving a slightly higher OLS. Unsurprisingly, the effect of muscle scattering is smallest for large ATT, as the relative photon path length in the muscle layer gets smaller with larger ATT.

The influence of the absorption coefficient μ_a on OLS is depicted in Fig. 8, where it is assumed that the absorption of the lipid layer is that of pure lipid added by a wavelength independent offset. The largest offset chosen here (0.006 mm^{-1}) is in the range of the likely muscle absorption coefficient and is much higher than what can be expected for adipose tissue. For this offset, the change in OLS is about 13% at the highest ATT.

For a comparison of the experimental findings shown in Figs. 1–5, the model was modified to take into account the finite resolution of the optical spectrometer employed for the

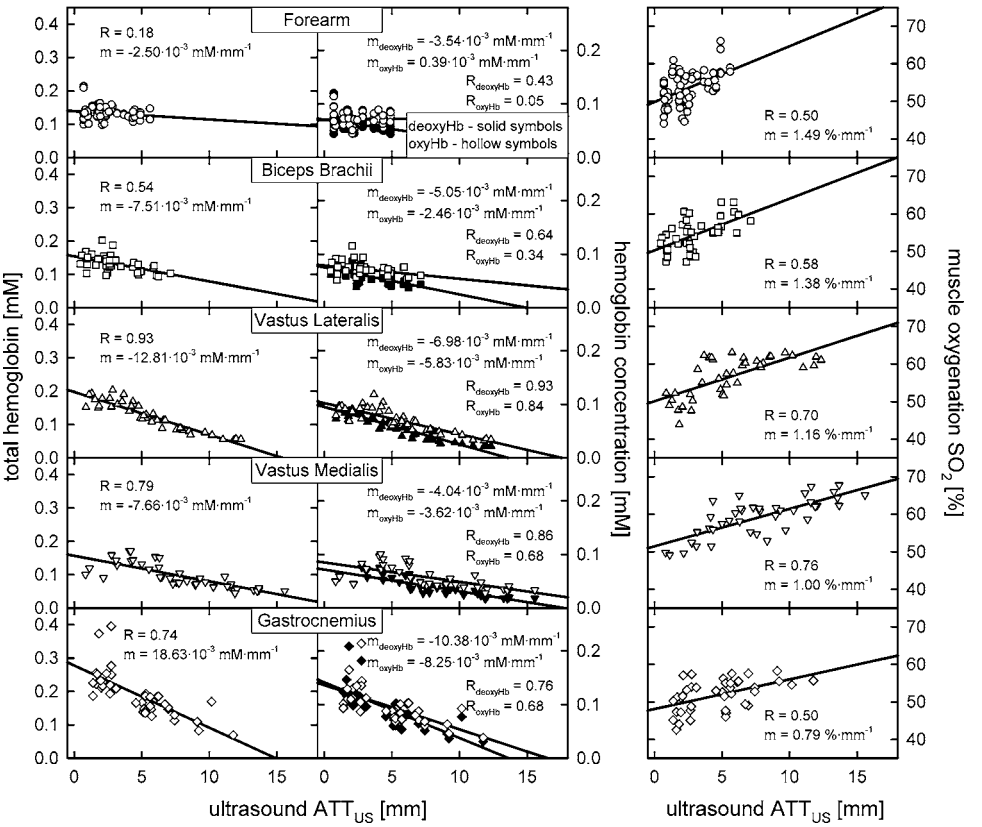

Fig. 6 Concentration of total hemoglobin tHb (left), deoxyHb (middle: solid symbols) and oxyHb (middle: open symbols), and oxygen saturation SO_2 (right) as a function of the adipose tissue thickness ATT_{US} (n=40 for each site). Values are separately plotted for the different muscle groups, with the correlation coefficient R and the slope m stated.

measurement of the attenuation spectra. To simulate this resolution, the modeled tissue reflectance spectra were smoothed by a gliding average filter with bandwidths of 1, 10, 15, and 20 nm [Fig. 8(b)]. To assess the agreement between experimental data and model, the most likely scattering and absorption properties have to be included. Here the following values were assumed: $\mu'_{s,M}$=0.7 mm^{-1}, $\mu'_{s,L}$=0.7 mm^{-1}, and $\mu_{a,\mathrm{Loffset}}$=0.002 mm^{-1}. Though these values are somewhat arbitrary, a vindication is given in Sec. 2. Furthermore, the absorption coefficient of the muscle layer was varied by a factor of 4 (μ_a=0.005–0.02 mm^{-1}). From the traces of Fig. 8(b), it is apparent that the effect of $\mu_{a,M}$ on the OLS versus ATT relationship is small, which again is explicable by the small photon path length in muscle. The larger bandwidth considerably reduces the OLS signal as the lipid absorption feature at 930 nm [compare with Fig. 1(c)] is smoothed. To allow a comparison with the experimental data, the 240 OLS values shown in Fig. 2(a) were grouped according to their corresponding ATT_{US} values, with equally spaced intervals of 1 mm. For each interval, the mean ($\pm$SD) of the experimental OLS values are plotted in Fig. 8(b). There is an overall agreement between the experimental data (spectrometer bandwidth $\approx$10 nm) and the model (for the modeled bandwidth =10 nm). However, it must be added that the uncertainties in the true scattering parameters of the lipid tissue have a large effect on the model predictions.

4 Discussion

With the work presented here, we follow and extend an earlier investigation by Conway, Norris, and Bodwell[18] and use the lipid absorption peak at about 930 nm by analysis of the second derivative of the attenuation spectra. A direct comparison with the data by Conway, Norris, and Bodwell is not feasible, as they compared the lipid signal with total body fat data rather than ATT, and details of their setup (e.g., bandwidth, source-detector distance) are not given. The reason for using the derivative of the spectra is that the background attenuation and crosstalk with other chromophores is reduced. Here we evaluated the ATT over five of the main skeletal muscle groups commonly studied with NIRS.

Correlation of optical lipid signal with ultrasound, calliper, and magnetic reasonance imaging. Our results show a strong correlation between the OLS and ultrasound measurement of ATT, indicating that the optical measure is a good indicator for ATT (Fig. 2). Though this might not be surprising, as lipid content is obviously linked to absorption, the significance of this finding is in the simplicity of the analysis, as no assumptions are made about the optical properties of tissue, the measurement geometry, the volume probed, or the hemoglobin content and oxygenation. OLS was found to be nonlinearly correlated with ATT (as measured by ultrasound, MRI, or calliper; Figs. 2–4 and Table 1), and this

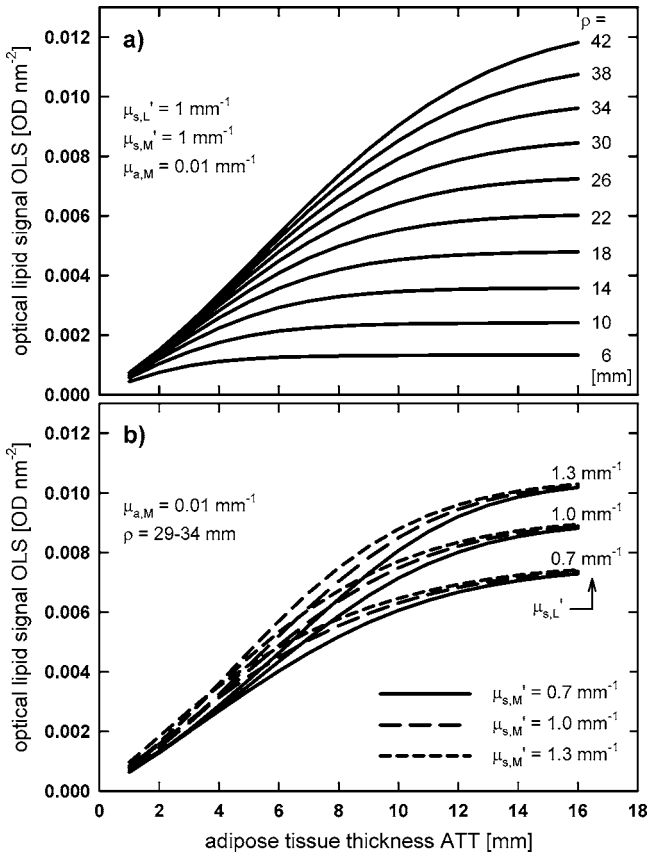

Fig. 7 OLS calculated from a two-layer tissue model (upper lipid layer: index L, lower muscle layer: index M) as a function of ATT. (a) Absorption coefficient of muscle was fixed at $\mu_{a,M}$=0.01 mm^{-1}, and the scattering coefficients of both layers were set to μ_s'=1 mm^{-1}. The source-detector distance ρ was varied from 6 to 42 mm. (b) OLS as a function of ATT for different scattering coefficients of both muscle and lipid layer by averaging over source-detector distances ρ from 29 to 34 mm.

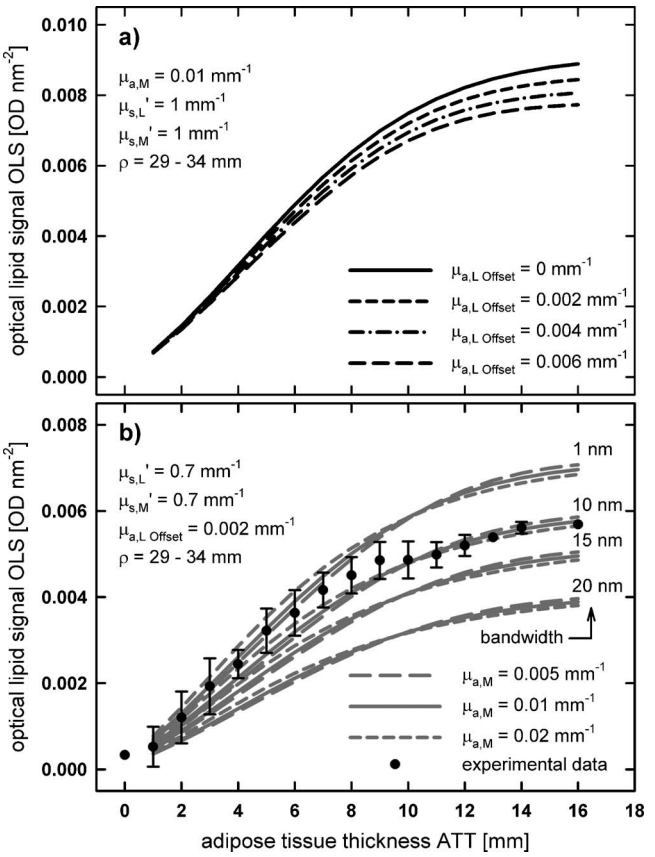

Fig. 8 (a) OLS for ρ=29 to 34 mm as function of ATT calculated for different levels of the absorption offset $\mu_{a,L,\text{offset}}$ in the lipid layer. In the model, the other parameters were fixed: $\mu_{a,M}$=0.01 mm^{-1}, $\mu_{s,L}'$ =1 mm^{-1}, $\mu_{s,M}'$=1 mm^{-1}, and ρ=29 to 34 mm. (b) Influence of muscle absorption coefficient $\mu_{a,M}$ on OLS when $\mu_{s,L}'$=0.7 mm^{-1}, $\mu_{s,M}'$=0.7 mm^{-1}, and $\mu_{a,L,\text{offset}}$=0.002 mm^{-1}. A spectrometer resolution of 1, 10, 15, and 20 nm was mimicked by spectral smoothing. The experimental values are based on the data shown in Fig. 2.

was confirmed by a theoretical, two-layer model (Figs. 7 and 8). When fitting an exponential equation [Eq. (4)] to the experimental data comparing OLS and ultrasound data (Fig. 2), a prediction error of ATT based on OLS was estimated to be about 0.84 mm or 28% when ATT data up to 16 mm were considered. This is comparable to optical versus MRI data (Fig. 4), though this is based on a different and smaller experimental dataset. Calliper readings were taken from the same sites as the ultrasound and OLS data: however, the elasticity and mechanical structure of skin prevented measurements to be obtained in about a quarter of the positions. For the remaining sites prediction errors and correlations with ultrasound data were larger than for OLS (Fig. 3 and Table 1). One source for errors is in the experimental inaccuracies both in determining ATT from ultrasound images and OLS from the optical attenuation spectra. These errors [experimental error bars in Fig. 2(a)] might explain a large part of the residuum. In conclusion, the data suggest that calliper readings are not found to be a reliable approach for the purpose of ATT determination, while OLS is a good predictor.

This finding is in contrast to published work where a poor correlation of ATT and optical signal measured with a commercial system was reported.[19–21] Here we can only speculate explanations, though there are a few noteworthy points. First, a likely explanation for the published rather poor correlation is the smaller source-detector distance of the instrument, which limits the sensitivity (compare Figs. 7 and 8). Second, the relationship between NIRS OLS signal and the other measurement modalities is nonlinear, and therefore the assessment of the validity on a standard (linear) correlation coefficient, as done in the literature, is flawed and a first approximation only. Third, to our knowledge there is no systematic published study validating the technical aspects like choice of wavelength, bandwidth, source-detector distance, and spectroscopic analysis.

Small crosstalk with hemoglobin. The crosstalk with hemoglobin changes was found to be small (Fig. 5), even when large variations of muscle oxygenation and hemoglobin concentration were induced by an exercise up to the maximal exercise power. The experimental data showed a coefficient of variation in OLS of about 4% over a time period of four hours and low correlation with hemoglobin oxygen saturation or attenuation. This low crosstalk with underlying absorption of both lipid and muscle tissue was confirmed in the model

(Figs. 7 and 8). This is comprehensible, as any absorption change with small wavelength variations at the lipid peak is removed by the second-derivative approach. This aspect is reassuring, as no simultaneous determination of hemoglobin is required and therefore the wavelengths might be restricted to a range of around 900 to 950 nm. Furthermore, in NIRS instrumentation, the optical ATT measurement can be done independently of hemoglobin measurements, which are usually based on wavelengths in the 700 to 850-nm range.

Source—detector geometry. The model presented in Fig. 7(a) suggests that the source-detector distance ρ should be at least twice the intended range of ATT measurements. For the experimental data of our study, the largest ATT_{US} was 16 mm and therefore at the limit of detectability with the equipment employed. From the six detector positions of the experimental system, only three were used. As for the three with larger distances (36.5, 39.0, and 41.5 mm), the signal was low and therefore the noise level high. The data indicate that for smaller ATT values, a smaller source-detector distance might be sufficient, and it seems advisable to adapt ρ to the ATT range. In the spectrometer setup employed here, the signal-to-noise ratio is rather critical, as the light intensity drops by about one order of magnitude for an increase of $\Delta\rho = 10$ mm, and the quantum efficiency of the CCD detector is fairly low for >900 nm. Furthermore, the nonlinearity of the OLS versus ATT relationship derived in the model is a direct outcome of the depth dependence of photon distribution, and it suggests that the prediction errors of ATT are larger for large ATT.

Dependence of tHb and SO_2 on adipose tissue thickness. For the body sites examined, the total hemoglobin concentration was found to decrease with ATT (Fig. 6). The physical explanation is the limited penetration depth into muscular tissue and its decrease with ATT. As the hemoglobin concentration of lipid is lower than for muscle, the apparent concentration as calculated by SRS is reduced. Similarly, SO_2 was found to increase with ATT (Fig. 6). These findings are similar to earlier results, though in the literature changes in hemoglobin or oxygen consumption and their dependence on ATT were evaluated.[6–8] In our data, the correlation of tHb with ATT was highest for the vastus lateralis and vastus medialis. The likely explanation is that these muscle groups are largest, and therefore the two-layer model is approximately valid. In the smaller muscles (forearm or biceps), the volume probed by the light might extend through the muscle to the bone, which might have different oxygenation parameters.

Comparison with a two-layer model. The comparison of the experimental data with the two-layer model (Fig. 7) relies on assumptions of a simplified model, i.e., mainly the absorption and scattering properties. As outlined in Sec. 2, literature values differ widely depending on the tissue interrogated, the experimental technique employed, and the analysis method used. In the model, the influence of $\mu'_{s,M}$ was tested and found to be small [Fig. 7(b)], which underpins the experimental findings of a low crosstalk with hemoglobin. Further concern is variations in the absorption coefficient of the adipose tissue, as no direct measurement is attempted here. A fair assumption is that the blood content of adipose tissue is considerably lower than that of muscular tissue, and therefore the contribution of hemoglobin to the absorption is insignificant. Its influence on the model was tested by adding an offset in μ_a [Fig. 7(a)], which is probably larger than the real value. The effect on the OLS versus ATT relationship was found to be small for small ATT, with increasing weight for larger ATT. Differences in the absorption coefficient of the muscle layer [Fig. 7(b)] were comparatively minute.

There are a number of obvious limitations to the model. First, the melanin absorption is neglected, which could be modeled as a third layer. Preliminary data from Monte Carlo simulations suggest the relative unimportance of this topic. Second, the layers were assumed to be homogeneous. Any nonhomogeneity might be modeled by Monte Carlo simulations,[36] though this would be futile without known geometry and exact optical properties. Third, for some smaller muscle groups, the photon penetration might reach beyond the muscle, and therefore a further layer simulating bone is needed. Furthermore, the scattering coefficient was assumed to be wavelength independent, though it drops by about $-0.5\cdot10^{-3}$ to $-1.0\cdot10^{-3}$ mm^{-1}/nm.[34,45] In a limited number of simulations, this effect was tested and found to be negligible. Another simplification and assumption is that the adipose tissue layer consists purely of lipid. Any deviation from this rough estimate does not affect the OLS versus ATT relationship but the model description.

5 Conclusion

From our data it can be concluded that NIR spectroscopy does provide the means to measure adipose tissue thickness, and this is shown for different body sites. This finding is in contrast to other studies in the literature and might be due to an appropriate experimental approach based on broadband spectroscopy. When taking ultrasound as a reference standard, the optical lipid signal compares favorably with calliper skin fold estimates and is comparable to MRI. The likely error is $<30\%$ or <0.8 mm. It must be stressed, however, that these findings are derived from a relatively young (mean age about 25 yrs) and healthy population, which might limit the conclusion for a broader population cross section. The optical lipid signal as a function of ATT can be described within a model of layered geometry, which provides advice on the appropriate source-detector geometry.

The significance of this finding depends on the objective. When aiming at ATT as the sole measurement parameter, ultrasound systems might be advisable, especially as recent systems are portable and lightweight. Though the spectroscopy system employed here is rather complex for widespread use, the potential advantage of optical systems is in size and simplicity. The main benefit of optical ATT quantification unfolds when combined with NIRS monitoring of hemoglobin, i.e., an all-optical system seems feasible for the monitoring of muscle oxygenation with an algorithm corrected for subcutaneous fat. So our vision is to merge recently developed algorithms that rely on the knowledge of ATT with the ATT measurement as described here.[9,16,53–55]

Acknowledgments

Alwin Kienle kindly supplied the program for the calculation of reflectivity of a two-layer model. The authors would like to

thank M. Klasing, A. Siegel, and J. Scholzen for acquiring the MR images. The work was supported by RheinAhrCampus Remagen.

References

1. M. Wolf, M. Ferrari, and V. Quaresima, "Progress of near-infrared spectroscopy and topography for brain and muscle clinical applications," *J. Biomed. Opt.* **12**(6), 062104 (2007).
2. V. Quaresima, R. Lepanto, and M. Ferrari, "The use of near infrared spectroscopy in sports medicine," *J. Sports Med. Phys. Fitness* **43**, 1–13 (2003).
3. Y. N. Bhambhani, "Muscle oxygenation trends during dynamic exercise measured by near infrared spectroscopy," *Can. J. Appl. Physiol.* **29**, 504–523 (2004).
4. S. Arridge, M. Cope, and D. T. Delpy, "The theoretical basis for the determination of optical pathlengths in tissue: temporal and frequency analysis," *Phys. Med. Biol.* **37**(7), 1531–1560 (1992).
5. M. S. Patterson, B. Chance, and B. C. Wilson, "Time resolved reflectance and transmittance for the non-invasive measurement of tissue optical properties," *Appl. Opt.* **28**(12), 2331–2336 (1989).
6. M. C. P. van Beekvelt, M. S. Borghuis, B. G. M. van Engelen, R. A. Wevers, and W. N. J. M. Colier, "Adipose tissue thickness affects in vivo quantitative near-IR spectroscopy in human skeletal muscle," *Clin. Sci.* **101**(1), 21–28 (2001).
7. W. Feng, D. Haishu, T. Fenghua, Z. Jun, X. Qing, and T. Xianwu, "Influence of overlying tissue and probe geometry on the sensitivity of a near-infrared tissue oximeter," *Physiol. Meas* **22**(1), 201–208 (2001).
8. T. Binzoni, C. Courvoisier, R. Giust, G. Tribillon, T. Gharbi, J. C. Hebden, T. S. Leung, J. Roux, and D. T. Delpy, "Anisotropic photon migration in human skeletal muscle," *Phys. Med. Biol.* **51**(5), 79–90 (2006).
9. L. Lin, M. Niwayama, T. Shiga, N. Kudo, M. Takahashi, and K. Yamamoto, "Influence of fat layer on muscle oxygenation measurement using near-IR spectroscopy: quantitative analysis based on two-layered phantom experiments and Monte Carlo simulation," *Front Med. Biol. Eng.* **10**(1), 43–58 (2000).
10. M. A. Franceschini, S. Fantini, L. A. Paunescu, J. S. Maier, and E. Gratton, "Influence of a superficial layer in the quantitative spectroscopic study of strongly scattering media," *Appl. Opt.* **37**(31), 7447–7458 (1998).
11. F. Martelli, A. Sassaroli, Y. Yamada, and G. Zaccanti, "Analytical approximate solutions of the time-domain diffusion equation in layered slabs," *J. Opt. Soc. Am. A* **19**(1), 71–80 (2002).
12. R. Nossal, J. Kiefer, G. H. Weiss, R. Bonner, H. Taitelbaum, and S. Havlin, "Photon migration in layer media," *Appl. Opt.* **27**, 33823391 (1988).
13. H. Taitelbaum, S. Havlin, and G. H. Weis, "Approximate theory of photon migration in a two-layer medium," *Appl. Opt.* **28**(12), 2245–2249 (1989).
14. A. H. Hielscher, H. Liu, B. Chance, F. K. Tittel, and S. L. Jacques, "Time-resolved photon emission from layered turbid media," *Appl. Opt.* **35**(4), 719–728 (1996).
15. J. M. Tualle, J. Prat, E. Tinet, and S. Avrillier, "Real-space Green's function calculation for the solution of the diffusion equation in stratified turbid media," *J. Opt. Soc. Am. A* **17**(11), 2046–2055 (2000).
16. D. Geraskin, H. Boeth, and M. Kohl-Bareis, "Spectroscopic measurement of adipose tissue thickness and comparison with ultrasound imaging," *Proc. SPIE* **6628**, 66281H (2007).
17. D. Geraskin, P. Platen, J. Franke, and M. Kohl-Bareis, "Algorithms for muscle oxygenation monitoring corrected for adipose tissue thickness," *Proc. SPIE* **6629**, 66290P (2007).
18. J. M. Conway, K. H. Norris, and C. E. Bodwell, "A new approach for the estimation of body composition: infrared interactance," *Am. J. Clin. Nutr.* **40**(6), 1123–1130 (1984).
19. N. J. Fuller, O. Dewit, and J. C. Wells, "The potential of near infrared interactance for predicting body composition in children," *Eur. J. Clin. Nutr.* **55**(11), 967–972 (2001).
20. K. Kalantar-Zadeh, E. Dunne, K. Nixon, K. Kahn, G. H. Lee, M. Kleiner, and F. C. Luft, "Near infra-red interactance for nutritional assessment of dialysis patients," *Nephrol. Dial Transplant* **14**(1), 169–175 (1999).
21. K. Brooke-Wavell, P. R. M. Jones, N. G. Norgan, and A. E. Hardman, "Evaluation of near infra-red interactance for assessment of subcutaneous and total body fat," *Eur. J. Clin. Nutr.* **49**(1), 57–65 (1995).
22. K. P. McLean and J. S. Skinner, "Validity of Futrex-5000 for body composition determination," *Med. Sci. Sports Exercise* **24**(2), 253–258 (1992).
23. P. J. Schreiner, J. Pitkäniemi, J. Pekkanen, and V. V. Salomaa, "Reliability of near-infrared interactance body fat assessment relative to standard anthropometric techniques," *J. Clin. Epidemiol.* **48**(11), 1361–1367 (1995).
24. V. L. Hicks, L. M. Stolarczyk, V. H. Heyward, and R. N. Baumgartner, "Validation of near-infrared interactance and skinfold methods for estimating body composition of American Indian women," *Med. Sci. Sports Exercise* **32**(2), 531–539 (2000).
25. J. R. Moon, S. E. Tobkin, A. T. Smith, M. D. Roberts, E. D. Ryan, V. J. Dalbo, C. M. Lockwood, A. A. Walter, J. T. Cramer, T. W. Beck, and J. R. Stout, "Percent body fat estimations in college men using field and laboratory methods: A three-compartment model approach," *Dyn. Med.* **7**, 7 (2008).
26. M. Elia, S. A. Parkinson, and E. Diaz, "Evaluation of near infra-red interactance as a method for predicting body composition," *Eur. J. Clin. Nutr.* **44**(2), 113–121 (1990).
27. R. A. Opplinger, R. R. Clark, and D. H. Nielsen, "New equations improve NIR prediction of body fat among high scholl wrestlers," *J. Orthop. Sports Phys. Ther.* **30**(9), 536–543 (2000).
28. D. W. Thomas, S. J. Ryde, P. A. Ali, J. L. Birks, C. J. Evans, N. H. Saunders, S. Al-Zeibak, J. Dutton, and D. A. Hancock, "The performance of an infra-red interactance instrument for assessing total body fat," *Physiol. Meas* **18**, 305–315 (1997).
29. Y. Sakurai, K. Nakamura, K. Teruya, N. Shimada, H. Matsuda, M. Sakurai, and S. Kono, "Comparison of percent body fat estimated by near infra-red spectrophotometry method with body mass index in health screening of male employees," *J. Epidemiol.* **4**(1), 47–50 (1994).
30. E. Tafeit, R. Möller, K. Sudi, and G. Reibnegger, "The determination of three subcutaneous adipose tissue compartments in non-insulin-dependent diabetes mellitus women with artificial neural networks and factor analysis," *Artif. Intell. Med.* **17**(2), 181–193 (1999).
31. E. Tafeit, R. Möller, K. Sudi, and G. Reibnegger, "Artificial neural networks as a method to improve the precision of subcutaneous adipose tissue thickness measurements by means of the optical device LIPOMETER," *Comput. Biol. Med.* **30**(6), 355–365 (2000).
32. R. Möller, E. Tafeit, K. H. Smolle, T. R. Pieber, O. Ipsiroglu, M. Duesse, C. Huemer, K. Sudi, and G. Reibnegger, "Estimating percentage total body fat and determining subcutaneous adipose tissue distribution with a new noninvasive optical device LIPOMETER," *Am. J.Hum. Biol.* **12**(2), 221–230 (2000).
33. B. Brooksby, B. W. Pogue, S. Jiang, H. Dehghani, S. Srinivasan, C. Kogel, T. D. Tosteson, J. Weaver, S. P. Poplack, and K. D. Paulsen, "Imaging breast adipose and fibroglandular tissue molecular signatures by using hybrid MRI-guided near-infrared spectral tomography," *Proc. Natl. Acad. Sci. U.S.A.* **103**(23), 8828–8833 (2006).
34. A. Torricelli, A. Pifferi, P. Taroni, C. D'Andrea, and R. Cubeddu, "In vivo multidistance multiwavelength time-resolved reflectance spectroscopy of layered tissues," *Proc. SPIE* **4250**, 290–295 (2001).
35. P. Taroni, D. Comelli, A. Farina, A. Pifferi, and A. Kienle, "Time-resolved diffuse optical spectroscopy of small tissue samples," *Opt. Express* **15**(6), 3301–3311 (2007).
36. E. Okada, M. Firbank, M. Schweiger, S. R. Arridge, M. Cope, and D. T. Delpy, "Theoretical and experimental investigation of near-infrared light propagation in a model of the adult head," *Appl. Opt.* **36**(1), 21–31 (1997).
37. T. J. Farrell, M. S. Patterson, and M. Essenpreis, "Influence of layered tissue architecture on estimates of tissue optical properties obtained from spatially resolved diffuse reflectometry," *Appl. Opt.* **37**(10), 1958–1972 (1998).
38. A. Kienle, M. S. Patterson, N. Dögnitz, R. Bays, G. Wagnières, and H. van den Bergh, "Noninvasive determination of the optical properties of two-layered turbid media," *Appl. Opt.* **37**(4), 779–791 (1998).
39. A. Kienle, T. Glanzmann, G. Wagnières, and H. van den Bergh, "Investigation of two-layered turbit media with time-resolved reflectance," *Appl. Opt.* **37**(28), 6852–6862 (1998).
40. D. Geraskin, P. Platen, J. Franke, and M. Kohl-Bareis, "Muscle oxygenation during exercise under hypoxic conditions assessed by spatially resolved broadband NIR spectroscopy," *Proc. SPIE* **5859**, 58590L, (2005).

41. R. L. P. van Veen, H. J. C. M. Sterenborg, A. Pifferi, A. Torricelli, E. Chikoidze, and R. Cubeddu, "Determination of visible near-IR absorption coefficients of mammalian fat using time- and spatially resolved diffuse reflectance and transmission spectroscopy," *J. Biomed. Opt.* **10**(5), 054004 (2005).
42. S. J. Matcher, P. Kirkpatrick, K. Nahid, M. Cope, and D. T. Delpy, "Absolute quantification method in tissue near infrared spectroscopy," *Proc. SPIE* **2389**, 486–495 (1995).
43. S. Suzuki, S. Takasaki, T. Ozaki, and Y. Kobayashi, "A tissue oxygenation monitor using NIR spatially resolved spectroscopy," *Proc. SPIE* **3597**, 582–592 (1999).
44. J. Soschinski, L. Ben Mine, D. Geraskin, G. Bennink, and M. Kohl-Bareis, "Cerebral oxygenation monitoring during cardiac bypass surgery in infants with broad band spatially resolved spectroscopy," *Proc. SPIE* **6629**, 66290U (2007).
45. S. J. Matcher, M. Cope, and D. T. Delpy, "In vivo measurements of the wavelength dependence of tissue-scattering coefficients between 760 and 900 nm measured with time-resolved spectroscopy," *Appl. Opt.* **36**(1), 386–396 (1997).
46. S. A. Prahl, "Tabulated molar extinction coefficient for hemoglobin in water," see http://omlc.ogi.edu/spectra/hemoglobin/summary.html (1998).
47. C. R. Simpson, M. Kohl, M. Essenpreis, and M. Cope, "Near-infrared optical properties of ex vivo human skin and subcutaneous tissues measured using the Monte Carlo inversion technique," *Phys. Med. Biol.* **43**(9), 2465–2478 (1998).
48. A. N. Bashkatov, E. A. Genina, V. I. Kochubey, and V. V. Tuchin, "Optical Properties of the Subcutaneous Adipose Tissue in the Spectral Range 400–2500 nm," *Opt. Spectrosc.* **99**(5), 836–842 (2005).
49. C. Casavola, L. A. Paunescu, S. Fantini, and E. Gratton, "Blood flow and oxygen consumption with near-infrared spectroscopy and venous occlusion: spatial maps and the effect of time and pressure of inflation," *J. Biomed. Opt.* **5**(3), 269–276 (2000).
50. P. Taroni, A. Pifferi, A. Torricelli, D. Comelli, and R. Cubeddu, "In vivo absorption and scattering spectroscopy of biological tissues," *Photochem. Photobiol.* **2**(2), 124–129 (2003).
51. L. Wang, S. L. Jacques, and L. Zheng, "MCML—Monte Carlo modelling of light transport in multi-layered tissues," *Comput. Methods Programs Biomed.* **47**(2), 131–146 (1995).
52. A. Kienle, Private communication (2007).
53. Y. Yang, M. R. Landry, O. O. Soyemi, M. A. Shear, D. S. Anunciacion, and B. R. Soller, "Simultaneous correction of the influence of skin color and fat on tissue spectroscopy by use of a two-distance fiber-optic probe and orthogonalization technique," *Opt. Lett.* **30**(17), 2269–2271 (2005).
54. Y. Yang, O. O. Soyemi, P. J. Scott, M. R. Landry, S. M. C. Lee, L. Stroud, and B. R. Soller, "Quantitative measurement of muscle oxygen saturation without influence from skin and fat using continuous-wave near infrared spectroscopy," *Opt. Express* **15**(21), 13715–13730 (2007).
55. K. J. Kek, R. Kibe, M. Niwayama, N. Kudo, and K. Yamamoto, "Optical imaging instrument for muscle oxygenation based on spatially resolved spectroscopy," *Opt. Express* **16**(22), 18173–18187 (2008).